

Comparison of OLI and TM Multi-spectral Satellite Imagery Land-use and Land-cover Mapping Using Hierarchical Concept of Earth Surface Matrix

Vahid rahdari*
Natural resource faculty, Isfahan university of technology, Isfahan, Iran
Natural resource faculty, University of Zabol, Zabol, Iran

Alireza Soffianian,
Natural resource faculty, Isfahan university of technology, Isfahan, Iran
Saeid Pormanafi,
Natural resource faculty, Isfahan university of technology, Isfahan, Iran

Razieh Mosadeghi,
Griffith university, Queensland Australia
Maxime Lenormand, Irstea, Montpellier, France

Abstract
The present study compares the capabilities of Thematic Mapper (TM) and Operational Land Imager (OLI) sensors of Landsat satellite and analyzes the results of image classification on their multi-spectral data. To achieve this, LANDSAT 5-TM (2011) and LANDSAT 8-OLI (2016) imageries were used to map the land-use and land-cover for a study area located on Pelasjan sub-basin, in Isfahan, Iran. First, radiometric and atmospheric corrections were performed, and then the overall status of the area was determined by reviewing topographic maps, visual interpretation of the satellite imageries and field studies. Consequently, a three-level land matrix hierarchy including 1) General level, 2) Mid-level, and 3) The level of details was established. Land matrix hierarchy maps were produced with proper methods using hybrid classification. The comparative analysis in this study showed that the hybrid classification method generates accurate results from the OLI sensor data in comparison to TM imageries. This was particularly evident for residential areas, irrigated agriculture, rain-fed agriculture, sparse, and dense rangelands. Although the results of image classification showed more accuracy for the OLI imagery, the error matrix in Z-test did not identify any statistically significant difference between the two datasets. This highlights the importance of image classification method selection, which can overcome the possible limitations of satellite imageries in land-use and land-cover mapping.
Keywords: OLI and TM Sensors, land matrix hierarchy, hybrid classification, LULC, error matrix.

1. Introduction

Land use land cover (LULC) mapping is typically based on remotely sensed data and image classification (Chrysoulakis et al. 2010; Kantakumar & Neelamsetti 2015) and plays an indispensable role in many LULC inventories, biodiversity conservation research, environmental modeling and … (Anderson 1976; Yu et al. 2014; Yu et al. 2015). There are several ways for producing LULC using remote sensing data (Purkis & Klemas 2011; Kantakumar and Neelamsetti 2015; Al-doski et al. 2013). In unsupervised classification, pixels were classified by paying attention to their digital number DN without field study (Balaji & Misra 2015). In supervised form, field observations are used to train a classifier to predict the LULC of an area from its spectral radiance or reflectance, texture (Purkis et al. 2006) and, in object-based classification, the shape, size and context of image segments (Blaschke 2010; Vieira et al. 2012; Phinn et al. 2012) but when land surface objects have similar reflectance or have small area most of them can't provide high accurate maps (Gao and Xu 2016).

Accurate LULC mapping needs proper data and image classification schemes. One of the main issues, when LULC maps are generated from digital images, is the confusion of spectral responses from different features (Estoque and Murayama 2015; Kntakumar and Neelamsetti 2015).

According to interference spectral reflectance of phenomena of the earth's surface in large scale, hierarchical image classification method can solve this problem. In this method, thematic maps of the earth surface from general to details will be produced by paying attention to the area characters and objects (Anderson 1976; Gregorio 2005; Homer et al. 2004; Disperati et al. 2015).

Landsat series of satellites are the most common Earth Observation (EO) data sources for LULC mapping (Malmir et al. 2015). Landsat Thematic Mapper (TM) started providing multispectral observations in 1984. Recently, with the launch of Landsat 8, carrying the Operational Land Imager (OLI) and the Thermal Infrared Sensor (TIRS), a new orthorectified dataset (L1T) became available (Roy et al. 2014; Knudbya et al. 2014; Kantakumar & Neelamsetti 2015). Having a nominal spatial resolution of 30 m, Landsat OLI, TIRS and TM

imagery are considered low resolution (LR) (Strahler et al. 1986) . Nevertheless, they can be used for mapping land surface, especially with complex landscape (Poursanidis et al. 2015).

By using low resolution imagery, land classification is challenging due to the spectral mixing of different surface elements and the landscape complexity (Julien et al. 2011; Stenzel et al. 2016). This is one of the main problems currently hampering the quantitative comparison of LULC maps by region or time period, even after time-consuming attempts at harmonization (Vancutsem et al. 2012; Disperati et al. 2015).

Hierarchical a-priori nomenclatures are the most robust and useful tools for LULC mapping (Di Gregorio 2005) over wide areas (i.e. at the scale of a country or larger) because they allow easier integration of data derived from different sources or different interpretation procedures. This concept also applies to multi temporal LULC analysis: maps related to different periods may accurately reveal changes only when they adopt the same nomenclature. Although alternative approaches such as hybrid, method can be useful for this purpose (Mirsa & Balaji 2015; Kantakumar & Neelamsetti 2015).

Several studies have also compared the obtainable accuracies between image classification methods and imageries' capability for producing accurate LULC maps (Benfield et al. 2007; Alves.V et al, 2012; Vieira et al. 2012; Al-doski et al. 2013; Knudbya et al. 2014; Estoque and Murayama 2015; Mei et al. 2015; Disperati et al. 2015; Poursanidis et al. 2015; Mirsa and Balaji 2015; Knudby et al. 2015).

The objective of this study is to compare the performance of Landsat 8 OLI against Landsat TM for LULC mapping in semi natural area mapping using best-designed method.

In this study, to reduce mixed pixel from different LULCs of Plasjan from Zayandehrood river sub-basin and sensors disability compensation, we applied a CORINE Land Cover (CLC) classification system to the study area and used a new hybrid classification scheme to develop TM and OLI sensors data.

The CLC system, prepared from national and European description, has proved to be an excellent decision-making support tool for environmental policy makers and spatial planners. (Feranec et al. 2007; Feranec al. 2010).

2. Materials and methods

2.1. Study area

The study is Pelasjan that is the sub-basin of Gavkhooni (Zayandehrood) basin located in the west of Isfahan Province in Iran 424,600 hectares area. It is located in 57˚49 to 47 ˚50 E and 16˚32 to 11 ˚ 33 north latitude. Figure 1 shows the location of the study in Gavkhooni Basin. This area has the highest share in water gains of the river. The area has diverse topography from plains to the high mountains, and is classified as cold and wet according to Domarton Method. Pelasjan area has small towns and villages, dams, rivers, soils, rangeland and rain-fed agricultural land areas covered with snow and mines (Matin et al. 2016).

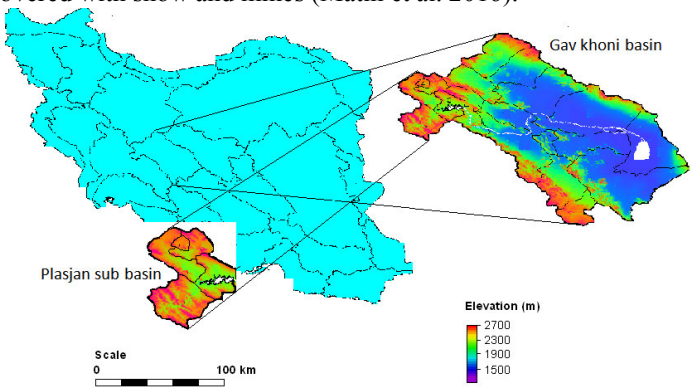

Figure 1. Pelasjan, located in the west part of the Zayandehrood Basin

2.2. Input data

Cloud free Landsat 5 TM sensor images acquired from August, June and February 2011, and June and August 2016 from Landsat 8 OLI sensor images were downloaded from the USGS website. Considering the fact that the study area was located between two columns, 164 and 165, two images were taken for each month.

Table1. Satellite imagery specification

Date of path	Satellite	Sensor	Sensor ID	Proc level	Pixel size
13-AUG-2011	Landsat	TM	Path/row 165/37	Ortho	30
06-AUG-2011	Landsat	TM	Path/row 164/37	Ortho	30
10-JUN-2011	Landsat	TM	Path/row 165/37	Ortho	30
03-JUN-2011	Landsat	TM	Path/row 164/37	Ortho	30
2-FEB-2011	Landsat	TM	Path/row 165/37	Ortho	30
09-JUN-15	Landsat	OLI	Path/row 165/37	Ortho	30
02-JUN-15	Landsat	OLI	Path/row 164/37	Ortho	30
12-AUG-15	Landsat	OLI	Path/row 165/37	Ortho	30
5-AUG-15	Landsat	OLI	Path/row 165/37	Ortho	30

Aerial photography, digital elevation model, topographic and pedological maps were also used. Field studies were also undertaken to capture training areas for each LULC class to be used in the image classification phase. Table 2 lists all the acquired data for this study.

Table2. Acquired data were used in the study

Data	Scale/Resolution	Source	Date
Topographic maps	(1/25,000)	Iran National Geographical Organization	2002
Historical aerial photo	(1/25,000)	National Cartographic Center, Iran	2010
Digital Elevation Model	(1/25,000)	National Cartographic Center, Iran	2014
Pedological maps	(1/25,000)	Isfahan University of Technology	2014
Satellite imagery	(1/50,000)	USGS web site	2016
Field studies			2016

2.3. LULC classification

Based on the available data and field studies, 10 LULC classes were defined for the study area (Table 3).

Table 3. LULC classification

	Class	Short description
1	Irrigated agriculture	Agricultural area, irrigated with rain and other sources of water
2	Rain-fed agriculture	agriculture area, irrigated only with rain water
3	Dense vegetation	vegetation cover crown more than 50% -natural vegetation upper than 50% and agriculture area
4	Sparse vegetation	Vegetation cover crown less than 50% and salinity less than 4 dSm
5	Residential area	Housing developments
6	Salt land	Vegetation cover crown less than 50% and salinity greater than 4 dSm
7	Stone and rock	Vegetation coverage less than 50% with more than 50% gravel
8	Water body	water bodies including; dam, natural and manmade lakes
9	Snow	Snow cover
10	Mine	Mining activities

Various cultivated crops' details are shown in table 4.

Table 4. Details about cultivation activitis in Pelasjan

Cod	Crope type	Cultivation and harvastion time
1	All wheat kinds	It is ciltvated in October and and has highest cover crown in first of Junary and harvested in mid Jully
2	Corn	It is ciltvated in June and has highest cover crown in Aguest, alsoit harvested in October
3	Alfalfa	It is ciltvated in the end of September and and has highest cover crown in the first of June
4	Potato	It is ciltvated in the end of June and has highest cover crown in the seecend half of August, also is harvested in Ocrober
5	Orchard	Time of leaf in early May and the fall in the second half of October

Random systematic sampling method was performed for each LULC class. Position of the lands under cultivation was determined with GPS. In addition, some information was prepared about cultivated crops density. Vegetation cover crown percentage (VCCP) sampling was done in areas with homogenous VCCP in at least nine 30 * 30 m adjacent. To check the status of the vegetation cover, 270 sampling areas and the vegetation cover crown was measured. VCCP was assessed using plots with 7 * 3 dimensions. Plot dimensions were determined using the Minimum Effective Area. To evaluate the accuracy of the maps, sampling was done on four percent of the number of pixels in each class. Saline soils, with more than 4 dSm salinity, were also mapped with 0.81 accuracy using

the data provided in a previous study carried out by Isfahan University of Technology in 2014.
In order to prepare the training site data for image classification, aerial photographs and interviews with local residents were used to validate the data.

2.4. Satellite image Pre-processing
The area was located in tow seen of imageries, and therefore for each date, images were mosaicked together by nearest neighbor method.

Radiometric correction was also applied on all the images using images Meta data in ENVI 5.1 software area. Images were atmospherically corrected using FLAASH (Fast Line-of-Sight Atmospheric Analysis of Spectral Hyper cubes) module. The output of this procedure is an image in apparent surface reflectance pixel units (resulting from rationing at-surface irradiance to at-surface radiance) (Kruse 2004).

2.5. Satellite image processing
2.5.1. Hierarchical mapping
At first, for image processing, the conceptual model of the three-level earth's surface matrix that was shown in Figure 2 was applied on both TM and OLI images.

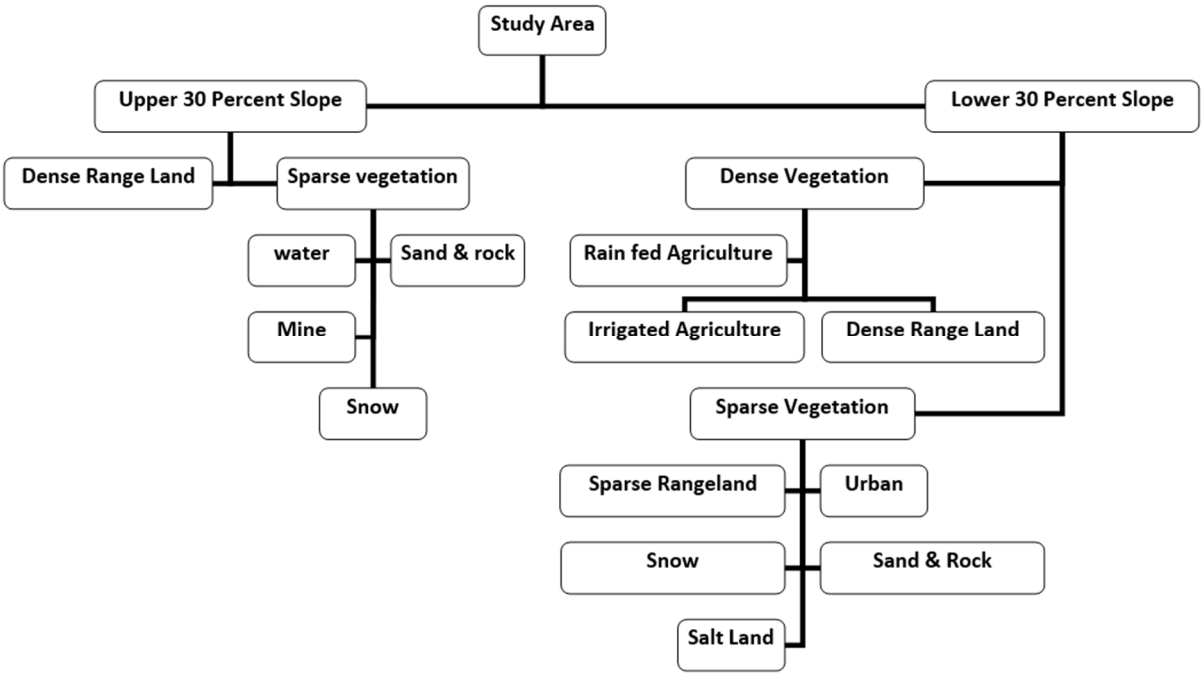

Fig.2 Hierarchical structure of Pelasjan matrix

First level mapping
By putting together, the visual interpretation of satellite images, field studies' results and slope layer, generated from the digital elevation model, it was determined that dense rangelands are often located in areas with slopes greater than 30 percent and, there is no agricultural activity in these areas. Thus, 30 percent threshold was used to map the first level at the hierarchical model (Figure 2).
Second level mapping

At this level, the lower CCP of rain-fed agriculture was considered as the threshold of 50% cover crown for separated dense vegetation (agriculture and dense rangeland) from sparse vegetation (sparse rangeland and other LULC). Consequently, in the second level of hierarchical model, dense vegetation and sparse vegetation were mapped for both slope classes identified in the first level.

One of the most common vegetation indices used in vegetation studies with satellite data is normalized difference vegetation index (NDVI), which has the ability to describe data from biophysical conditions of the plants such as fractional cover, condition, and the plant biomass (Mie et al. 2015; Estoque & Murayama 2015). To map VCCP, NDVI index was used as follows (Formula: 1):

$$\text{NDVI} = \frac{NIR - RED}{NIR + RED}$$

Where NIR is band 5 in and RED is band 5, band 4 in OLI sensor, also band 4, and band 3 in TM sensor, respectively.

Using 250 VCCP measurements' sampling results, simple linear regression was done between samples taken as the dependent variable, and their NDVI values for each image as independent variable. Using prepared VCCP models, the VCCP maps were prepared in two levels. Because the less CCP in rain-fed agriculture was 50 percent, it was determined as threshold for dense and separate vegetation, then threshold value of 50% in NDVI index was used to classify the vegetation coverages with less or more than 50% cover crown.

Third level mapping

On the third level of the hierarchical model (Figure 2), three categories of irrigated, rain-fed agriculture and dense rangeland were considered as the sub-classes for the dense vegetation (>50% vegetation coverage). Seven categories were also determined as the sub-classes for the low-density vegetation (<50%) including residential areas, sparse rangeland, land under water, stone and gravel, soils, mines, and land under snow. In the third level mapping, dense mountain rangeland map was provided by overlaying area with more than 30 percent slope on dense vegetation map provided in level 2. In addition, the Fisher supervise classification was performed on areas with a slope more than 30 and less than 50 VCCP images; and areas with stone and gravel, snow, mining areas, waterbody areas were mapped. The remaining pixels, which were not in this class, were considered as low-density rangelands.

In areas with lower than 30% slope, in both TM and OLI sensor imageries, irrigated agriculture was mapped using Fisher method. In OLI images, rain-fed agricultural areas were separated from rangeland using Fisher classification method. In TM images, it could not be possible to separate rain-fed agriculture from rangeland accurately; therefore, they were separated using Object-Based Classification method of rangeland due to their geometric shape. Moreover, for separating dense rangeland from irrigated agriculture, this method was used.

After separating agricultural lands from others, using VCCP models, sparse rangeland was separated from dense rangeland for each date.

For the June 2016 imagery using OLI imagery, in areas with lower 30% slope, all the other layers, mining activity areas, residential areas, water body, salt land, stone and rock, and snow were generated by applying Fisher supervised classification method.

For the TM imagery, first and second level mapping were generated following similar steps undertaken for the June 2016 imagery. Lands covered by snow, water, and salt were mapped using Fisher method. Residential areas were identified using the Jan 2011 imagery, when the ground was completely covered with snow using band-6 TM imagery. Thus, the threshold value of residential areas without snow and desert areas covered with snow was determined, and then by applying the reclassification method, these layers were mapped. The mining area was mapped manually through visual assessment using Digital Viewer.

Finally, all the individual layers were combined, and consequently, of the LULC, maps were generated using the hybrid classification methods described in the previous sections.

2.6. Maps accuracy assessment

To assess the accuracy of the research method, the capabilities of each sensor in producing the LULC maps, four percent of the identified classes in the third level maps were collected as polygon data. We were ensured that the samples were reflective of all the different land cover classes. Additionally, to validate the generated maps, field samples, aerial photographs, and interpretation of FCC images, community consultation and matrix of error were used. The overall accuracy and Kappa coefficient, producer accuracy, user accuracy, commission error and omission were also determined.

3. Results and discussion

Understanding surface reflectance patterns is useful in accreted mapping. In this study, some details about each LULC reflectance were obtained using clustering supervised classification.

Image classifications' results have shown that LULC classes with the same reflectance values in different bands have more errors. Moreover, small patches of isolated land covers can also increase the classification errors because of impact of the reflections from the adjacent pixels (Luna & Cesar 2003; Yuan et al. 2005; Kamusoko & Aniya 2007; Kantakumar & Neelamsetti 2015; Estoque & Murayama 2015). Therefore, the accuracy of the classification in unsupervised methods depends on the degree of differentiation among the spectral reflections of LULC (Kamusoko & Aniya 2007).

Residential areas that were small patches were distributed across the study area, and therefore their reflectance was influenced by the neighboring pixels.

Although Fisher classification method was able to separate the residential areas in both sensors, in some cases, residential areas and low-density rangeland were classified as one class in TM sensor images.

Figures 3a and 3b show the spectral graph of each land cover class in Landsat TM and OLI sensors, respectively. As shown in the figures, the residential areas, low-density rangelands and even rain-fed lands follow a very similar reflectance pattern in all bands of the sensors.

Note: the values presented in the chart are average values for each LULC class.

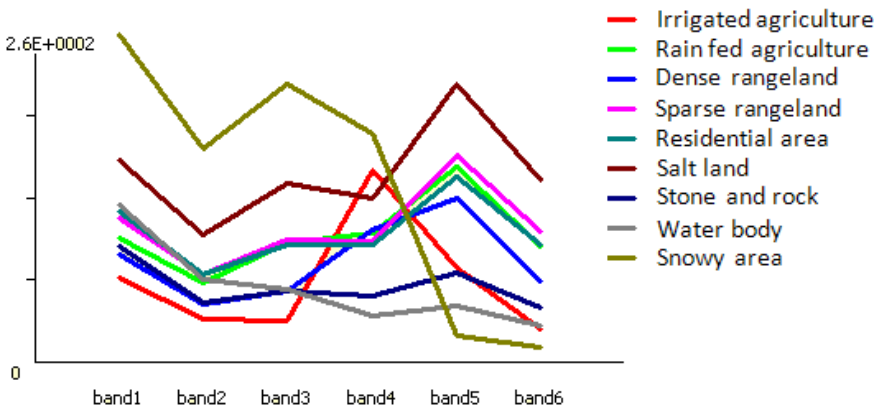

Fig. 3a, An example of the spectral profile for TM sensor

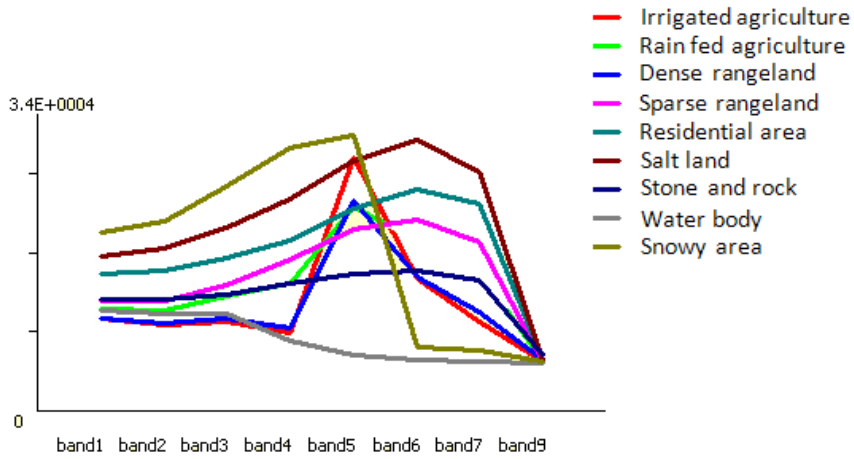

Fig. 3b, An example of the spectral profile for OLI sensor

Because of radiometric resolution, in the OLI sensor, reflectances of different phenomena are more distinguishable. This distinction leads to more accurate classification results using the OLI sensor (Estoque & Murayama 2015). The error matrix table below provides more details on the above-mentioned classification errors. Given the physical characteristics of water and snow, the reflectance for these land cover classes were easily distinguishable and were mapped with higher accuracy.

For separating lower and more than 50 VCCP, models were prepared for each imagery, and formulae 2 and 3 have shown the VCCP model.

Equivalent 2: $Y = 179.3X + 24.89$ $R^2 = 0.89$ P-value < 0.01 for 2016

Equivalent 3: $Y = 2\ 40.95x + 16.13$ $R^2 = 0.80$ P-value < 0.01 for 2011

Where Y is VCCP, X is values in NDVI index.

The field sampling and overlaying false color images on gradient map also indicated that dense rangelands are normally located on slopes greater than 30 percent, while irrigated and rain-fed farming were located on slopes less than 30 percent slope. Thus, by applying the slope layer on the satellite images, dense rangeland ranges were separated.

Finally, LULC map was defined using the conceptual model and with hybrid method for the area in 10 layers for January 2016 and 2011. Figures 5 and 6, a and b show LULC maps of the area in the second and third stages. The area is shown in hectares and the total area ratio of the area of each class is shown in table 5.

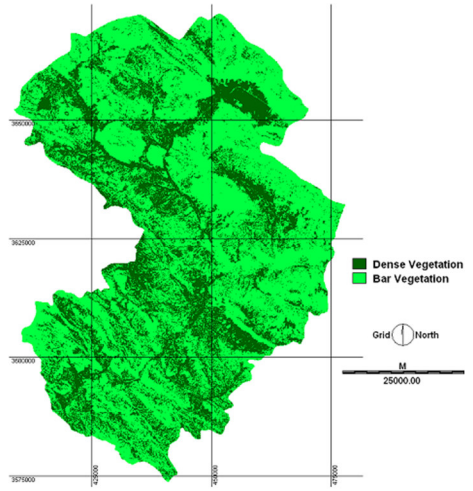

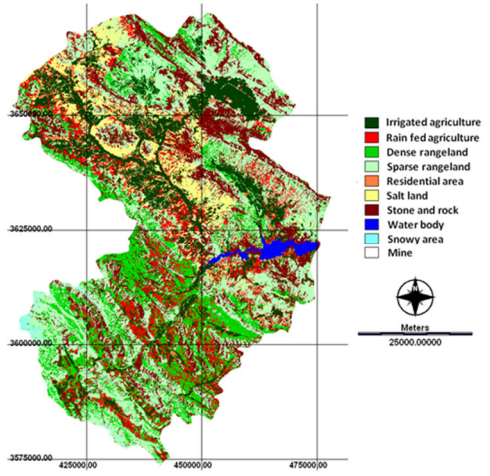

Fig 5.a, Dense and sparse vegetation for 2011

Fig 5.bLULC map for 2011

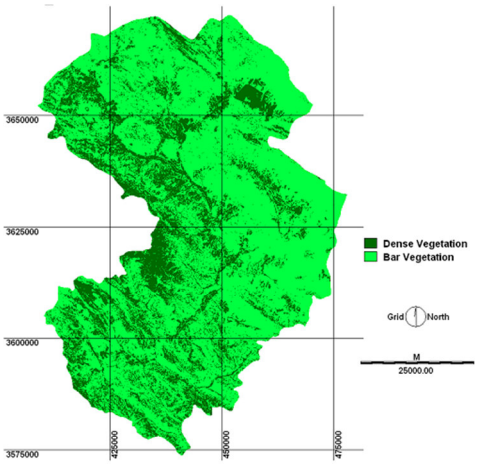

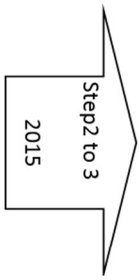

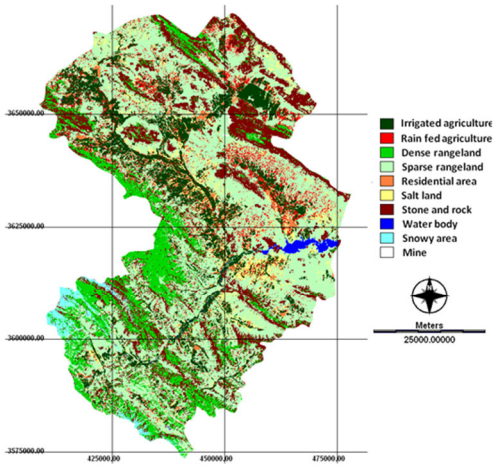

Fig 6.a, Dense and sparse vegetation for 2016

Fig 6.b, LULC map for 2016

Table 5. Plasjan sub basin LULC area (Hectare)

LULC code / Area	1	2	3	4	5	6	7	8	9	10
Area 2011	15	1571	4336	66288	28590	2800	131519	68884	46604	66245
Area 2016	156	6101	3670	67932	21386	4110	179639	53380	25511	58054

Maps' accuracy assessment was done with re-sampling and using data that were not used in the analysis. Error Matrix of the final map of 2011 related to TM sensor and 2016 OLI sensor produced, and kappa coefficient, overall accuracy, precision of producer and user, commission and omission errors were calculated and shown in Tables 6 and 7.

Table 6. LULC error matrix for TM image 2011

	1	2	3	4	5	6	7	8	9	10	User Accuracy	Error O
1	25573	994	423	615	53	1	0	0	0	27659	0.925	0.075
2	203	10126	329	292	2	310	0	0	0	11262	0.899	0.101
3	28	48	21724	50	0	180	166	0	2	22198	0.979	0.021
4	13	170	1036	76802	1	1299	199	0	0	79520	0.966	0.034
5	0	0	0	0	1785	2	0	0	0	1787	0.999	0.001
6	2	63	29	1639	2	7787	0	0	0	9522	0.818	0.182
7	0	0	205	317	0	0	27184	0	1	27707	0.995	0.018
8	0	0	0	0	0	0	0	1183	0	1183	1.000	0.000
9	0	0	0	1	0	0	0	0	2714	2715	1.000	0.000
10	25819	11401	23746	79716	1843	9579	27549	1183	2717	183553		
Producer accuracy	0.998	0.804	0.956	0.985	0.979	0.695	0.994	1.000	0.997	Corrected pixels		
Error C	0.009	0.112	0.085	0.036	0.031	0.187	0.013	0.000	0.001	174878		
Kappa Coefficient	0.936											
Overall accuracy	0.952											

Table 7. LULC error matrix for OLI image 2016

Land use/cover	1	2	3	4	5	6	7	8	9	10	User Accuracy	Error O
1	28728	3748	1594	16	88	12	0	0	0	34186	0.840	0.160
2	352	14891	1078	187	7	644	0	0	0	17159	0.868	0.132
3	51	871	24980	1580	12	1139	443	0	0	29076	0.859	0.141
4	34	104	2188	55997	4	1849	743	0	5	60924	0.919	0.081
5	0	35	0	0	1488	0	0	0	0	1523	0.977	0.023
6	0	52	0	189	2	9046	1	0	0	9290	0.974	0.026
7	0	34	9	453	6	9	28253	0	15	28779	0.982	0.018
8	0	0	0	0	0	0	0	1927	0	1927	1.000	0.000
9	0	0	0	0	0	0	10	0	679	689	0985	0.015
10	29165	19735	29859	58422	1607	12699	29450	1927	699	183553		
Producer accuracy	0.985	0.755	0.837	0.958	0.926	0.712	0.959	1.000	0.971	Corrected pixels		
Error C	0.015	0.245	0.163	0.042	0.074	0.288	0.041	0.000	0.029	165989		
Kappa Coefficient	0.880											
Overall accuracy	0.904											

As shown in tables 6 and 7, irrigated agricultures were separated correctly from other LULC using Fisher classification method in both imageries. Tables 6 and 7 show that most errors are related to relating rain-fed area and dense rangeland to irrigated agricultural. Due to their similar nature in dense areas, these two land uses have similar reflectance characteristics close to irrigated agriculture (fig 3a and 3b), and some pixels of dense dryland farming have a DN close to dense peripheral irrigated areas' pixels. For this reason, corrected separation of the two layers, using an 8-bit image of TM sensor, was not possible.

Error matrix obtained from the two sensors indicates that in the map prepared by OLI sensor image, rain-fed agriculture, irrigated agriculture and dense and sparse rangeland were separated correctly. However, eventually misclassified pixels in produced maps using OLI images in irrigated agriculture, rain-fed and dense rangeland existed.

Due to the small size of residential areas in the study area, it is not possible to provide accurate maps using TM images. Field measurements have shown that human activities have made these areas warmer than peripheral areas. The TM image corresponding to the period when the area was covered with heavy snow for February has shown that residential areas did not have snow cover after some days.

In prepared maps, some irrigated agricultural pixels in both images are wrongly related to residential areas because of small green spaces in residential areas.

The highest errors on the maps were in attributing low-density rangeland and saline soils to each other because of similarities in provided hierarchical structure, definitions, and similar reflection of these two layers in some areas due to the change in vegetation cover crown of these layers. Thus, in some saline lands with an increase in the percentage of the vegetation cover, they were related to low-density rangeland. Water and snowy body's maps in both TM and OLI sensor images were prepared with high accuracy, which is due to different reflecting behaviors of water compared to other phenomena (FIG 3 a and 3b).

4. Conclusion

Today, several remote sensing data from satellites and various sensors are available to users. Landsat satellites have different sensors such as MSS, TM, ETM + and recently OLI. TM is a useful sensor with a resolution of 8-bit radiometric on Landsat 5, and OLI sensor is the newest generation of Landsat sensors on Landsat 8 with 16-bit radiometric resolution (Peña & Brenning 2015).

Results have shown that LULC area and spectral distance are affected on accurate mapping; also in this study classical methods could not provide accurate maps (Stenzel et al. 2016). In hybrid method that were used different methods such as fisher supervised classification, object based classification, NDVI index and Slope layer and also was carried out step by step, more accurate LULC maps were produced (Al-doski et al. 2013). However, the results have shown that even this method was not able to produce a map with overall accuracy of more than 80 percent. Therefore, by attention to field studies, characteristics of the land and capabilities of the sensors were tried to prepare final LULC maps in the third stages. Therefore, LULC maps of the area were possible by combining hybrid classification method and hierarchy concept of land matrix. In this study, Fisher classification method for the separation of residential areas and object-based classification method for separating rain-fed agricultural areas were carried out from rangeland.

More radiometric resolution of OLI sensor, and the youthfulness of this sensor compared to TM sensor enabled better separation of ground-level phenomena. Figures 3a and 3b show that although some phenomena in the Landsat TM images have similar reflectance behaviors to OLI, the numerical distance between graphs has been raised in the OLI sensor graphs making it possible to separate some LULCs, which were close to each other in Landsat TM.

Maps' accuracy, assessed using samples that were not used in the analysis of satellite images, led to the prevention of false increased accuracy of the maps provided due to using these data.

Error matrices show that the mean and variance of classified map by Landsat TM and OLI are not significant in any of the rows and columns. However, statistical analysis T-TEST has shown predictable excellence in the map provided by OLI sensor, especially in mapping different vegetation types and separating land surfaces such as residential areas. However, lack of significant difference is due to the methods used that had been prepared for each image regarding area status.

Considering the similarity of reflecting land phenomena in this study, the existence of some features such as residential areas with relatively small areas, and by considering reflective similarities and the hierarchy concept of matrix, hybrid method was used. Thus, the possibility of providing detailed maps of LULC areas that have small areas with reflective interference with other phenomena was provided through appropriate methods for each of the classes defined for both sensors.

References

- Al-doski, J., Shattri, M & Zulhaidi M.S, H. (2013), "Image classification in remote sensing» Journal of Environment and Earth Science, 3 (10), 141-147.
- Akgun, A., Eronat, A.H & Turk, N. (2012), "Comparing different satellite image classification methods: an application in Ayvalik district, western Turkey", Landslides journal (9), 1, 93-106.
- Anderson, J.R. (1976), "A Land Use and Land Cover Classification System for Use with Remote Sensor Data", U.S. Government Printing Office.
- Benfield, S.L., Guzman, H.M., Mair, J.M & Young, J.A.T. (2007), "Mapping the distribution of coral reefs and associated sublittoral habitats in Pacific Panama: a comparison of optical satellite sensors and classification methodologies", International Journal of Remote Sensing (28), 5047–5070.
- Blaschke, T. (2010), "Object based image analysis for remote sensing", ISPRS Journal of Photogrammetry and Remote Sensing (65), 2–16.
- Chander, G., Markham, B.L & Helder, D.L. (2009), "Summary of current radiometric calibration coefficients for Landsat MSS, TM, ETM+, and EO-1 ALI sensors", Remote Sens. Environ. 113, 893–903. http://dx.doi.org/10.1016/j.rse.2009.01.007.
- Chrysoulakis, N., Abrams, M., Feidas, H & Korei, A. (2010), "Comparison of methods using ASTER data for the area of Crete, Greece", Int. J. (31), 6347–6385.
- Darvishsefat, A. (1999), "Thematic GIS Data based Maps Accuracy Assessment", 5th Geographic Information System conference.
- Di Gregorio, A. (2005), "Land cover classification system classification concepts and user manual software version (2) ", In FAO environment and natural resources service series, no. 8. Rome: Food and Agriculture Organization of the United Nations.
- Disperati, L., Gonario, S & Virdis, P. (2015), "Assessment of land-use and land-cover changes from 1965 to 2014 in Tam Giang-Cau Hai Lagoon, central Vietnam", Applied Geography (58), 48-64.
- Estoque, R.C & Murayama, Y. (2015), "Classification and change detection of built-up lands from Landsat-7 ETM+ and Landsat-8 OLI/TIRS imageries: A comparative assessment of various spectral

indices", Ecological Indicators journal (56), 205-217.
- Feranec, J., Hazeu, G., Christensen, S., & Jaffrain, G. (2007), "CORINE land cover change detection in Europe (case studies of the Netherlands and Slovakia) ", Land Use POLIcy 24(1), 234-247.
- Feranec, J., Jaffrain, G., Soukup, T., & Hazeu, G. (2010), "Determining changes and flows in European landscapes 1990e2000 using CORINE land cover data", Applied Geography (30), 19-35.
- Gao, J & Xu, L. (2016), "An efficient method to solve the classification problem for remote sensing image", AEU - International Journal of Electronics and Communications (69), 1, 198–205
- Homer, C., Huang, C., Yang, L., Wylie, B., & Coan, M. (2004), "Development of a 2001 national land cover database for the United States", Photogrammetric Engineering and Remote Sensing, 70(7), 829e840.
- Julien, Y., Sobrino, J.A & Jiménez-Mu˜noz, J.C. (2011), "Land use classification from multitemporal Landsat imagery using the Yearly Land Cover Dynamics (YLCD) method", International Journal of Applied Earth Observation & Geoinformation (13), 711–720
- Kamusoko, C., Aniya, M. (2007), "Land use/cover change and landscape fragmentation analysis in the Bindura District, Zimbabwe", Land Degradation&Development, 18(2), 221–233.
- Kantakumar, L.N & Neelamsetti, P. (2015), "Multi-temporal land use classification using hybrid approach", The Egyptian Journal of Remote Sensing and Space Sciences (18), 2, Pages 289–295.
- Knudby, A., Mtwana.N, L., Palmqvistc, G., Wikströmc, K., KOLIji, A., Lindborgd, R & Gullströmc, M. (2014), "Using multiple Landsat scenes in an ensemble classifier reduces classification error in a stable nearshore environment", International Journal of Applied Earth Observation and Geoinformation (28), 90–101.
- Kruse A.F. (2004), "Comparison of ATREM, ACORN, & FLAASH aTMospheric corrections using low-altitude AVIRIS data of Boulder", Presented at the JPL Airborne Geoscience Workshop, CA: Jet Propulsion Laboratory, Pasadena.
- Lobo, F., Costa, M.P.F & Novo, E.M(2015), "Time-series analysis of Landsat-MSS/TM/OLI images over Amazonian waters impacted by gold mining activities", Remote Sensing of Environment 157, 170–184.
- Luna,A.R & Cesar,A.R. (2003), "Land use, land cover changes and costal lagoon surface reduction associated with urban growth in northwest Mexico", Landscape Ecology, (18),159-171.
- Lunetta, R.S & Lyon, J.G. (2004), "Remote Sensing and GIS Accuracy Assessment", CRC Press.
- Malmir, M., Kheirkhah.Z, M.M., Monavari, S.M., Jozi, S.A & Sharifi, S. (2015), "Urban development change detection based on Multi-Temporal Satellite Images as a fast tracking approach-a case study of Ahwaz County", southwestern Iran. Environ Monit Assess (187),3, 187- 108.
- Mahmoud, M., Yazdani, M.R & Bahman.P, M. (2006), "Assessment and management of soil erosion in Zayandeh rood basin (Gav khoni), The first regional conference of proper use of water in Gav khoni and Karon basin, Share kord, Shahre kord university.
- Mei, A., Ciro, M., Fontinovo, M., Bassani, A.A & Petracchini, F. (2015), "Landsat 8 vs. Landsat 5: A comparison based on urban and peri-urbanland cover mapping Dimitris", Journal of African Earth Sciences, Article in press.
- Misra, R & Balaji, R. (2015), "A study on the shoreline changes and Land-use/ land-cover along the South Gujarat coastline", Procedia Engineering 116, 381 – 389
- Nurdin, N., Teruhisa, T., Agus, M.A., Djalil1, A.R and Khairul, A. (2015), "Multisensor & Multitemporal Data from Landsat Images to Detect Damage to Coral Reefs, Small Islands in the Spermonde Archipelago, Indonesia", Ocean Science journal 50(2), 317-325.
- Oldeland, J., Dorigo, W., Lieckfeld, L., Lucieer, A & Jurgens, N. (2010), "Combining vegetation indices, constrained ordination and Fuzzy classification for mapping semi-natural vegetation units from hyperspectral imagery", Remote sensing environment (114), 1155-1166.
- Peña, M.A and Brenning, A. (2015), "Assessing fruit-tree crop classification from Landsat-8 time series for the Maipo Valley, Chile", Remote Sensing of Environment (171), 234–244.
- Phinn, S.R., Roelfsema, C.M & Mumby, P.J. (2012), "Multi-scale, object-based image analysis for mapping geomorphic and ecological zones on coral reefs", International Journal of Remote Sensing (33), 3768–3797.
- Poursanidis, D., Chrysoulakis, N & Mitraka, Z. (2015), "Landsat 8 vs. Landsat 5: A comparison based on urban and peri-urbanland cover mapping", International Journal of Applied Earth Observation and Geoinformation (35), 259–269.
- Purkis, S.J & Klemas, V.V. (2011), "Remote Sensing and Global Environmental Change", John Wiley & Sons.
- Purkis, S., Myint, S & Riegl, B. (2006), "Enhanced detection of the coral Acropora cervicornis from satellite imagery using a textural operator", Remote Sensing of Environment (101), 82–94.
- Roy, D.P. (2014), "Landsat-8: science and product vision for terrestrial global change research", Remote

Sens. Environ. 145 (5), 154–172.

- Stenzel, S., Ewald. F, F and Mack, B & Schmidtliein, S. (2016), "Identification of high nature value grassland with remote sensing and minimal field data", Ecological Indicators (74), 28–38.
- Tian, B., Zhou, Y.X., Thom, R.M., Diefenderfer, H.L & Yuan, Q. (2015), " Detecting wetland changes in Shanghai, China using FORMOSAT and Landsat TM imagery", Journal of Hydrology (529), 1–10
- Tucker, C.J., Grant, D.M & Dykstra, J.D. (2004), "NASA's global orthorectified Landsatdata set. Photogramm", Eng. Remote Sens. (70), 313–322.
- Vancutsem, C., Marinho, E., Kayitakire, F., See, L & Fritz, S. (2012), "Harmonizing and combining existing land cover/land use datasets for cropland area monitoring at the African continental scale", Remote Sensing, 5(1), 19-41.
- Vieira, M.A., Formaggio, A.R., Rennó, C.D, Atzberger, C., Aguiar, D.A & Mello, M.P. (2012), "Object Based Image Analysis and Data Mining applied to a remotely sensed Landsat time-series to map sugarcane over large areas", Remote Sensing of Environment (123), 553–56.
- Yuan, F., Sawaya, K.E., Loeffelholz, B.C & Bauer, M.E. (2005), "Land cover classification and change analysis of the twin Cities (Minnesota) metropOLItan area by multitemporal Landsat remote sensing", Remote sensing of Environment (98), 317-328.